AGU PUBLICATIONS

JGR

Journal of Geophysical Research: Space Physics

RESEARCH ARTICLE
10.1002/2016JA022429

Key Points:
- Temperature anisotropy instabilities in space plasma
- Effects of proton to electron mass ratio in particle-in-cell simulations of the proton mirror instability
- Effects of electron temperature anisotropy on the growth and saturation of proton cyclotron and proton mirror instabilities

Correspondence to:
N. Ahmadi,
narges.ahmadi@unh.edu

Citation:
Ahmadi, N., K. Germaschewski, and J. Raeder (2016), Effects of electron temperature anisotropy on proton mirror instability evolution, *J. Geophys. Res. Space Physics*, *121*, doi:10.1002/2016JA022429.

Received 24 JAN 2016
Accepted 26 APR 2016
Accepted article online 2 MAY 2016

Effects of electron temperature anisotropy on proton mirror instability evolution

Narges Ahmadi[1], Kai Germaschewski[2], and Joachim Raeder[2]

[1]Department of Physics, University of New Hampshire, Durham, New Hampshire, USA, [2]Department of Physics and Space Science Center, University of New Hampshire, Durham, New Hampshire, USA

Abstract Proton mirror modes are large amplitude nonpropagating structures frequently observed in the magnetosheath. It has been suggested that electron temperature anisotropy can enhance the proton mirror instability growth rate while leaving the proton cyclotron instability largely unaffected, therefore causing the proton mirror instability to dominate the proton cyclotron instability in Earth's magnetosheath. Here we use particle-in-cell simulations to investigate the electron temperature anisotropy effects on proton mirror instability evolution. Contrary to the hypothesis, electron temperature anisotropy leads to excitement of the electron whistler instability. Our results show that the electron whistler instability grows much faster than the proton mirror instability and quickly consumes the electron-free energy so that there is no electron temperature anisotropy left to significantly impact the evolution of the proton mirror instability.

1. Introduction

There is a region of the dayside magnetosheath which is characterized by temperature anisotropy $T_\perp/T_\parallel > 1$, where $T_\perp$ and $T_\parallel$ indicates the perpendicular and parallel temperatures relative to the background magnetic field B_0, respectively. The temperature anisotropy is caused by plasma heating at the quasi-perpendicular bow shock and field line draping close to the magnetopause as shown by *Midgeley and Davis* [1963] and by *Zwan and Wolf* [1976]. This temperature anisotropy leads to the generation of low-frequency waves. For $T_{p\perp}/T_{p\parallel} > 1$, where T_p shows proton temperature, proton cyclotron waves [*Kennel and Petscheck*, 1966] and proton mirror waves [*Chandrasekhar et al.*, 1958; *Hasegawa*, 1969] are generated, and for $T_{e\perp}/T_{e\parallel} > 1$, where T_e stands for electron temperature, electron whistler waves [*Kennel and Petscheck*, 1966; *Scharer and Trivelpiece*, 1967] and electron mirror waves [*Gary and Karimabadi*, 2006] can grow.

The proton cyclotron instability is a resonant instability, and it propagates parallel to the background magnetic field with frequencies less than the proton gyrofrequency ($\omega < \Omega_p$), while the proton mirror instability has zero frequency ($\omega = 0$) in a homogeneous plasma in the plasma frame, and its wave vector is oblique to the background magnetic field. Here Ω_p denotes the proton gyrofrequency. The mirror instability creates magnetic depressions or magnetic mirrors in the plasma, which can trap particles, and in this way, particles exchange their kinetic energy to the wave and instability grows, as shown by *Southwood and Kivelson* [1993]. Linear theory predicts that mirror modes are more likely to be dominant in high $\beta_{p||}$ regions of the magnetosheath while proton cyclotron modes are dominant in the low $\beta_{p||}$ plasma conditions, where $\beta_{p||}$ is the ratio between parallel proton pressure to magnetic pressure [*Gary*, 1992].

The electron whistler waves propagate parallel to the background magnetic field with frequencies larger than proton gyrofrequency and smaller than electron gyrofrequency ($\Omega_p < \omega < \Omega_e$), where Ω_e is the electron gyrofrequency. The electron mirror instability is similar to the proton mirror instability, but its wavelength is of the order of electron inertial length ($d_e = c/\omega_{pe}$). All of these instabilities compete with each other to consume the available free energy of the system which is contained in the temperature anisotropies. Proton cyclotron and proton mirror instabilities compete with each other for the available free energy in proton temperature anisotropy while electron whistler and electron mirror instabilities compete for consuming the electron temperature anisotropy. But there is also a competition between proton mirror instability and electron whistler instability to consume the available electron-free energy which we are interested to study in this paper.

There are frequent observations of proton mirror mode structures in the Earth's magnetosheath [*Kaufmann et al.*, 1970; *Tsurutani et al.*, 1982]. Proton mirror modes have also been observed in the solar wind [*Winterhalter et al.*, 1995], at comets [*Russell et al.*, 1987], in the magnetosheaths of other planets like Jupiter and Saturn

[*Erdos and Balogh*, 1996; *Bavassano-Cattaneo*, 1998; *Joy et al.*, 2006], and in the heliosheath [*Burlaga et al.*, 2006]. Proton mirror modes have been observed in regions with low proton plasma beta $\beta_{p||}$, although the linear dispersion theory predicts that proton cyclotron mode should be the dominant mode in these regions.

Price et al. [1986] showed that the presence of heavy ions tends to suppress the proton cyclotron instability while the growth rate of the proton mirror instability is not significantly affected. This can be one possible mechanism for proton mirror modes to dominate proton cyclotron instability [*Gary*, 1992; *Gary et al.*, 1993]. *Shoji et al.* [2009] performed two- and three-dimensional hybrid simulations to study the competition between these two modes. They suggested that in three-dimensional simulations, proton mirror modes consume most of the free energy of the system and it stops the growth of the proton cyclotron waves. *Porazik and Johnson* [2013a] used the gyrokinetic theory to derive the linear dispersion relation for the proton mirror instability and provided a coherent view of different kinetic approaches that is used to obtain the dispersion relation. They also used gyrokinetic approach to simulate the nonlinear development of the mirror instability [*Porazik and Johnson*, 2013b]. *Seough and Yoon* [2013] suggested that temporal or spatial variations in the magnetic field strength, which affect the resonance condition for the proton cyclotron instability but do not affect the resonance condition for the proton mirror instability, may also suppress the proton cyclotron instability.

The purpose of this work is to study the effects of electron temperature anisotropy on the evolution of proton mirror instability. Linear dispersion theory shows that the electron temperature anisotropy enhances the proton mirror instability growth rate, but it does not affect the proton cyclotron instability growth rate significantly [*Gary*, 1992].

Since we need to consider electron dynamics, we use particle-in-cell (PIC) simulations to include kinetic effects of both protons and electrons. Electrons get anisotropically heated in the shock layer similar to protons [*Burgess et al.*, 2012]. Some previous studies have assumed electrons to be isotropic, since they performed hybrid simulations which treats electrons as a fluid [*Shoji et al.*, 2009; *Hellinger et al.*, 2005]. However, *Tsurutani et al.* [1982] have shown that the electron temperature anisotropy is generally larger than 1 in Earth's magnetosheath.

Masood and Schwartz [2008] analyzed Cluster data in Earth's magnetosheath and found that electrons exhibit significant temperature anisotropy in the deep magnetosheath due to magnetic field line draping while being isotropic downstream of the quasi-perpendicular bow shock. *Pokhotelov et al.* [2000, 2001, 2002] developed a linear theory to study the effects of finite electron temperature on proton mirror instability threshold, and they confirmed that for sufficiently hot electrons, the proton mirror instability growth rate is enhanced. *Remya et al.* [2013] used linear theory to study the role of electron temperature anisotropy on the proton cyclotron and proton mirror instabilities, and they conclude that an inclusion of anisotropic electrons with $T_{e\perp}/T_{e||} \geq 1.2$ reduces the proton cyclotron growth rate substantially and increases the proton mirror instability growth rate. However, they did not consider the presence of the electron whistler instability.

In section 2, we solve the linear dispersion relation to find the growth rates of the instabilities for given plasma parameters. In section 3, we benchmark our kinetic code with linear dispersion theory for both proton temperature anisotropy and electron temperature anisotropy instabilities. In section 4, we present simulation results for different proton to electron mass ratios and how electron anisotropy affects the growth of the proton mirror instability. In section 5, we discuss the conclusions.

2. Linear Analysis

We solved the linear dispersion relation for a homogeneous, collisionless plasma with bi-Maxwellian distributions to measure the growth rates of the temperature anisotropy instabilities for typical magnetosheath plasma parameters. We consider two species: protons and electrons. We assume charge neutrality $n_p = n_e$ and zero relative drift between the electrons and protons [*Stix*, 1962]. Solutions of the linear dispersion equation are typically expressed in terms of dimensionless variables. It is natural to use electron inertial length and electron gyrofrequency as normalizing factors for electrons and proton inertial length and proton gyrofrequency for normalizing proton-related instabilities.

In Earth's magnetosheath, the distributions become anisotropic because of heating of the particles across the quasi-perpendicular bow shock and field line draping. The time scale of the heating through the shock is about one proton gyroperiod. This time scale is very fast and does not allow the proton instabilities to grow

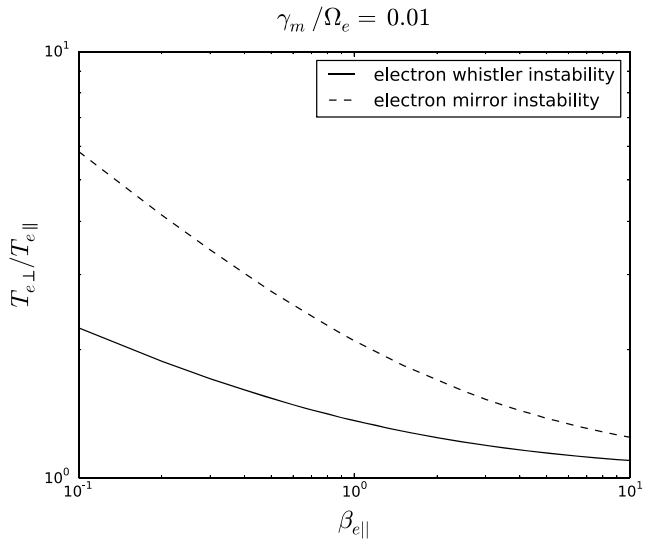

Figure 1. Electron temperature anisotropy at the $\gamma_m/\Omega_e = 0.01$ thresholds of electron whistler and electron mirror instabilities as function of $\beta_{e||}$. The solid line shows the instability threshold of electron whistler instability, and the dashed line shows the electron mirror instability threshold. If the plasma parameters lie below the threshold line, the instabilities growth rate will be smaller than the threshold.

in the shock layer. Therefore, a considerable amount of proton temperature anisotropy persists downstream of the quasi-perpendicular shock in the magnetosheath. For electrons, on the other hand, one proton gyroperiod equals 1836 electron gyroperiods. Thus, electron instabilities have sufficient time to grow and isotropize the electron distributions. Therefore, we consider high proton temperature anisotropies and lower electron temperature anisotropies to resemble the magnetosheath plasma conditions downstream of the quasi-perpendicular shock [*Burgess et al.*, 2012].

2.1. Competition Between Electron Whistler and Electron Mirror Instability

Figure 1 shows the instability thresholds for electron whistler and electron mirror instabilities. We keep $T_{p\perp}/T_{p||} = 1$ and $\beta_{p||} = 1$. The instability thresholds ($\gamma_m/\Omega_e = 0.01$) are measured using linear dispersion theory. The γ_m refers to maximum growth rate. Comparing the electron whistler and electron mirror instability growth rates in Figure 1, we clearly see that the electron whistler instability has a lower instability threshold than the electron mirror instability, and it may therefore suppress the electron mirror mode. Observations [*Gary et al.*, 2005] show that electrons follow the marginal stability path of the electron whistler instability in Earth's magnetosheath, which indicates that electron whistler instability is the dominant instability. *Gary and Wang* [1996] provided an analytical instability threshold for electron whistler instability. The threshold condition for $\gamma_m/\Omega_e = 0.01$ is

$$R_w = \beta_{e||}^{0.55}\left(\frac{T_{e\perp}}{T_{e||}} - 1\right) \geq 0.36 \tag{1}$$

$R_w \geq 0.36$ means plasma is unstable relative to electron whistler instability and for $R_w < 0.36$ plasma is electron whistler stable.

2.2. Competition Between Proton Cyclotron and Proton Mirror Instability

In the case of the proton temperature anisotropy instabilities, the proton cyclotron instability has larger growth rate compared to the proton mirror instability for low proton plasma beta $\beta_{p||}$ and it should be the dominant instability in the magnetosheath as shown in Figure 2. The analytical threshold condition for the proton mirror instability in a homogeneous plasma with warm anisotropic electrons is given by *Pantellini and Schwartz* [1995] and *Pokhotelov et al.* [2000],

$$R_m = \beta_{p\perp}\left(\frac{T_{p\perp}}{T_{p||}} - 1\right) + \beta_{e\perp}\left(\frac{T_{e\perp}}{T_{e||}} - 1\right) - \frac{\beta_{e||}}{2}\frac{\left(\frac{T_{p\perp}}{T_{p||}} - \frac{T_{e\perp}}{T_{e||}}\right)^2}{1 + \frac{T_{e||}}{T_{p||}}} \geq 1 \tag{2}$$

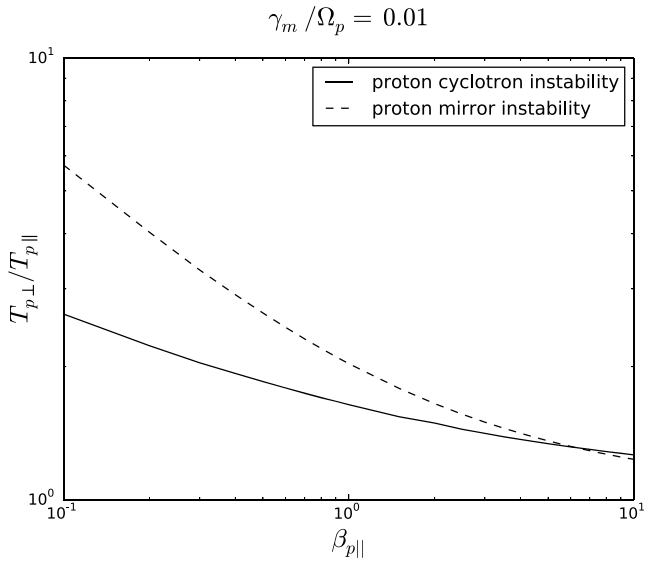

Figure 2. Proton temperature anisotropy at the $\gamma_m/\Omega_p = 0.01$ thresholds of proton cyclotron and proton mirror instabilities as function of $\beta_{p||}$. The solid line shows the instability threshold for proton cyclotron instability, and the dashed line shows the proton mirror instability threshold. If the plasma parameters lie below the threshold line, the instabilities growth rate will be smaller than the threshold.

and for proton cyclotron instability the analytical threshold of the instability is [*Gary and Lee*, 1994]

$$R_p = \beta_{p||}^{0.42}\left(\frac{T_{p\perp}}{T_{p||}} - 1\right) \geq 0.43 \tag{3}$$

We use these threshold conditions to determine which instability is dominant in our simulations. In Figure 2, we keep electrons isotropic and measure the proton cyclotron and mirror instability thresholds ($\gamma_m/\Omega_p = 0.01$) using linear dispersion theory. It is clear that the proton cyclotron instability has larger growth rate compared to mirror instability for low $\beta_{p||}$ and high $T_{p\perp}/T_{p||}$. But observations [*Joy et al.*, 2006; *Soucek et al.*, 2008; *Génot et al.*, 2009; *Balikhin et al.*, 2010; *Tsurutani et al.*, 2011; *Seough and Yoon*, 2013] show that in regions where we expect the dominance of the proton cyclotron instability, mirror instability has grown and it is the dominant mode. So the question is, what helps the proton mirror instability to grow faster than the proton cyclotron instability in low $\beta_{p||}$ regions?

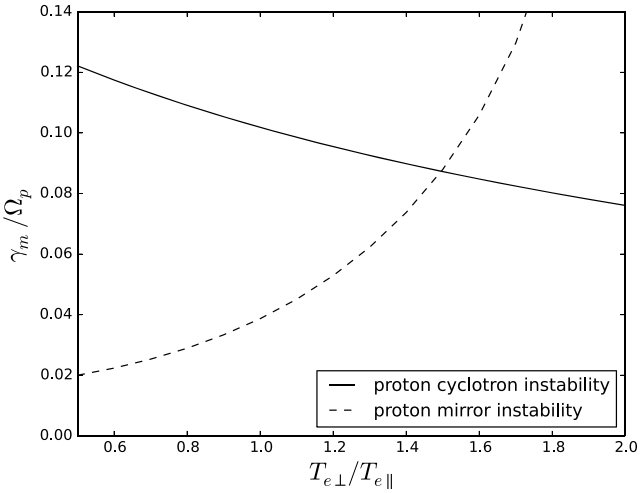

Figure 3. Electron temperature anisotropy effects on mirror and proton cyclotron instability maximum growth rates. Solid line shows the maximum growth rate of the proton cyclotron instability as a function of electron temperature anisotropy, and dashed line shows the maximum growth rate of proton mirror instability. $T_{p\perp}/T_{p||} = 2.5$ and $\beta_{p||} = \beta_{e||} = 1$ are fixed.

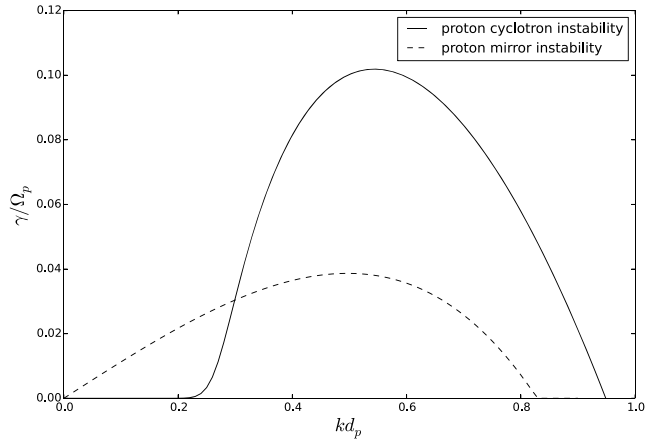

Figure 4. The growth rate as a function of wave number for proton cyclotron and proton mirror instability. Solid line shows the proton cyclotron instability growth rate at $\theta_m = 0$ while the dashed line shows the growth rate of proton mirror instability at $\theta_m = 63$. The maximum growth rate of proton cyclotron instability is $\gamma_m/\Omega_p = 0.10$ at $k_m d_p = 0.54$ with $\omega_r/\Omega_p = 0.52$ while the proton mirror instability maximum growth rate is $\gamma_m/\Omega_p = 0.039$ with $k_m d_p = 0.5$.

One possibility is the effects of electron temperature anisotropy on the proton mirror instability growth rate. Figure 3 shows that by increasing the electron temperature anisotropy, mirror instability growth rate increases while leaving the proton cyclotron instability only slightly affected. The reason is that proton cyclotron instability is a resonant instability and electrons do not resonate with the proton cyclotron mode, but they can get trapped in the magnetic bottles of the mirror instability and exchange energy with the wave.

In order to study the nonlinear effects of the electron dynamics on the evolution of the proton mirror instability, we use PIC simulations.

3. Verification of PSC by Comparison to Linear Dispersion Theory

PSC is a state of the art electromagnetic PIC simulations code described by *Germaschewski et al.* [2013]. In this section, we compare the PSC results with linear dispersion theory. In order to show that PSC can capture temperature anisotropy instabilities correctly, we measured the growth rate of the instabilities from simulation in the linear regime for selected plasma parameters and compare with linear theory predictions.

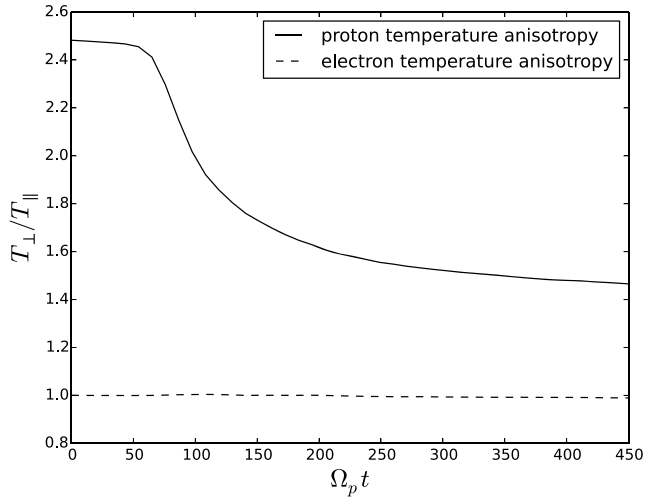

Figure 5. Proton and electron temperature anisotropy evolution as a function of time in 2-D particle in cell simulation. Initial parameters are $T_{p\perp}/T_{p\parallel} = 2.5$, $T_{e\perp}/T_{e\parallel} = 1$, and $\beta_{p||} = \beta_{e||} = 1$. The linear regime of proton temperature anisotropy instabilities is about $\Omega_p t = 70$.

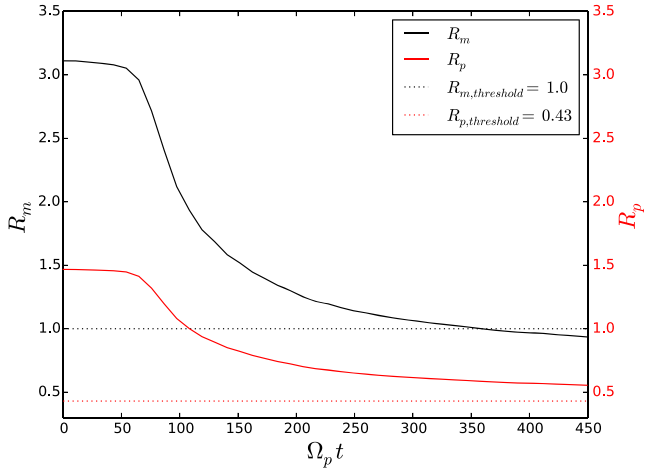

Figure 6. Proton cyclotron and proton mirror instabilities threshold conditions as a function of time. Plasma follows the proton cyclotron instability threshold at the nonlinear regime. Initial parameters are $T_{p\perp}/T_{p\|} = 2.5$, $T_{e\perp}/T_{e\|} = 1$, and $\beta_{p||} = \beta_{e||} = 1$.

We start with bi-Maxwellian protons and Maxwellian electrons. We choose $T_{p\perp}/T_{p\|} = 2.5$, $T_{e\perp}/T_{e\|} = 1$, and $\beta_{p||} = \beta_{e||} = 1$. We perform two-dimensional simulations with $L_y = L_z = 128d_p$ where L_y and L_z are the length of the simulation box in y and z directions, ω_p is the proton plasma frequency, and $d_p = c/\omega_p$ is the proton inertial length. The number of grid points ($n_y \times n_z$) is 4096×4096. Periodic boundary conditions are used in both dimensions. A constant background magnetic field $\mathbf{B_0}$ is assumed in the z direction.

With anisotropic protons ($T_{p\perp}/T_{p||} > 1$), proton cyclotron and proton mirror instabilities will grow. From linear theory, we expect the maximum growth rate of the proton cyclotron instability to be $\gamma_m = 0.10\Omega_p$ at $k_m d_p = 0.54$ and θ=0° while the proton mirror instability maximum growth rate is $\gamma_m = 0.039\Omega_p$ with $k_m d_p = 0.50$ at θ=63° as shown in Figure 4. The θ is the angle between the wave number vector $\mathbf{k}$ and $\mathbf{B_0}$. Figure 5 shows the temperature anisotropy evolution of both protons and electrons. We calculate the temperatures by averaging it over the entire simulation domain. Electrons remain isotropic. As proton cyclotron and proton mirror instabilities start growing, the proton temperature anisotropy decreases. The linear regime of the proton temperature anisotropy instabilities extends through about $\Omega_p t = 70$ in this case. Figure 6 shows the instability thresholds for both proton cyclotron and proton mirror instability measured by equations (2) and (3). It is clear that plasma follows the proton cyclotron instability threshold condition. Figures 7 and 8

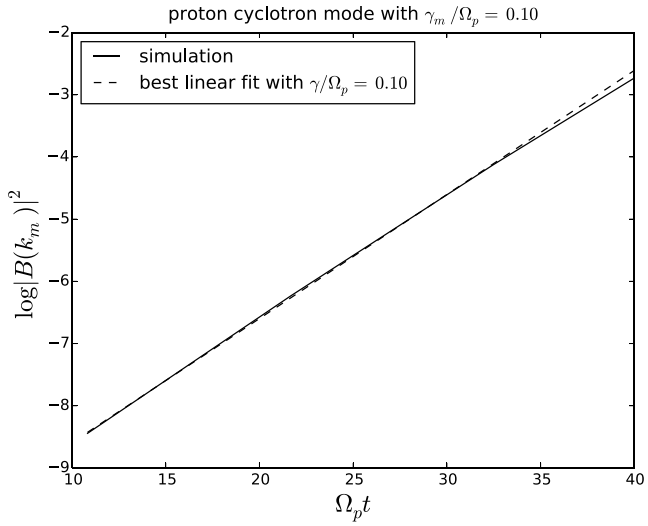

Figure 7. Measured maximum growth rate of proton cyclotron instability from simulation in the linear regime. The measured growth rate is in agreement with linear dispersion theory prediction.

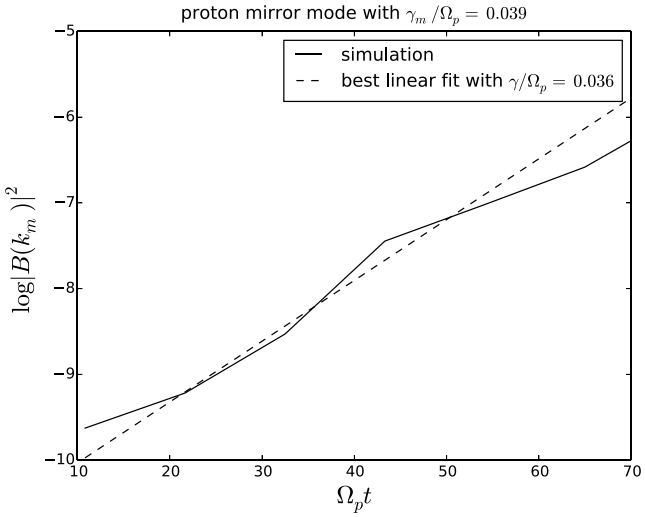

Figure 8. Measured maximum growth rate of proton mirror instability from simulation in the linear regime. The measured growth rate is in good agreement with linear dispersion theory prediction.

compare the measured maximum growth rate of proton cyclotron and proton mirror instabilities from simulation with linear dispersion theory predictions. The simulation results are in good agreement with linear theory.

We perform a similar benchmarking simulation for electron whistler and electron mirror instabilities to show that we are resolving the electron physics in our simulations. Here we choose $T_{p\perp}/T_{p\parallel} = 1$, $T_{e\perp}/T_{e\parallel} = 2$, and $\beta_{p||} = \beta_{e||} = 1$ and otherwise the same parameters as in the previous case. Now with anisotropic electrons ($T_{e\perp}/T_{e||} > 1$), electron whistler and electron mirror instability grow. Figure 9 shows the growth rate of electron whistler and electron mirror instabilities as a function of wave number k. For the given plasma parameters, linear dispersion theory predicts that the maximum growth rate of the electron whistler instability is $\gamma_m = 0.10\Omega_e$ at $k_m d_e = 0.64$ with $\omega_r/\Omega_e = 0.36$ and θ=0° while electron mirror instability has a maximum growth rate of $\gamma_m = 0.006\Omega_e$ at $k_m d_e = 0.37$ and θ=73°. Figure 10 shows the temperature anisotropy evolution and the electron whistler instability threshold condition according to equation (1). The proton distribution stays in equilibrium and isotropic. The electron temperature anisotropy instabilities consume the electron-free energy and isotropize the electrons. The linear regime of the electron whistler instability lasts

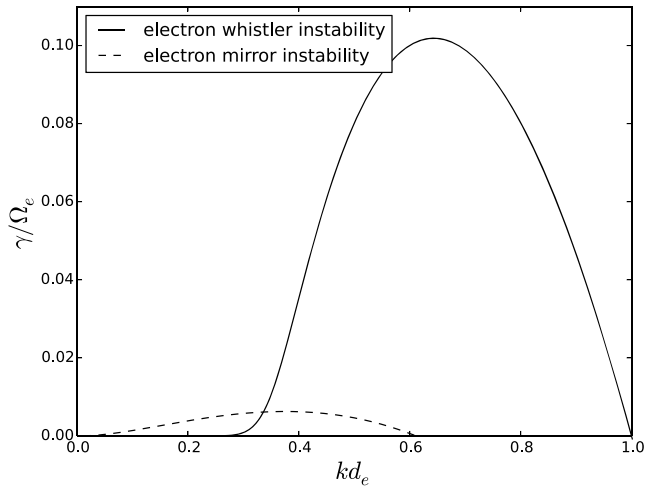

Figure 9. The growth rate as a function of wave number for electron whistler and electron mirror instability. Solid line shows the electron whistler instability growth rate at $\theta_m = 0$ while the dashed line shows the growth rate of electron mirror instability at $\theta_m = 73$. The maximum growth rate of electron whistler instability is $\gamma_m/\Omega_e = 0.10$ at $k_m d_e = 0.64$ with $\omega_r/\Omega_e = 0.36$ while the electron mirror instability maximum growth rate is $\gamma_m/\Omega_e = 0.006$ with $k_m d_e = 0.37$.

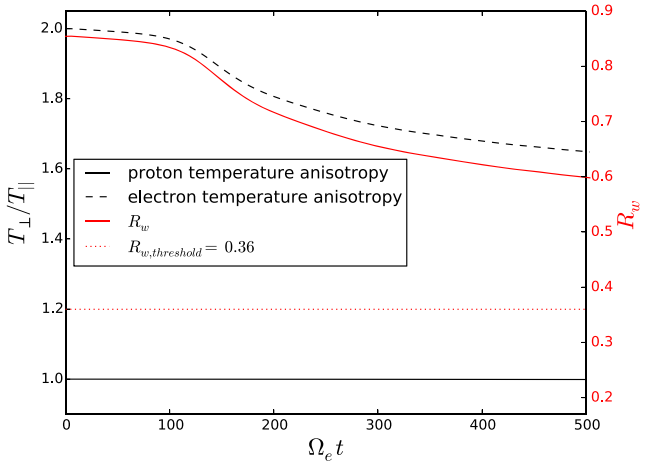

Figure 10. Proton and electron temperature anisotropies evolution and the electron whistler instability threshold condition as a function of time in 2-D particle-in-cell simulation. Initial parameters are $T_{p\perp}/T_{p\parallel} = 1$, $T_{e\perp}/T_{e\parallel} = 2$ and $\beta_{p||} = \beta_{e||} = 1$.

to about $\Omega_e t = 20$, while the linear regime of electron mirror instability would extend to $\Omega_e t = 250$ since electron mirror instability maximum growth rate is about 17 times smaller than the electron whistler instability maximum growth rate. Figures 11 and 12 show the comparisons of the measured growth rates from simulation with linear dispersion theory predictions. We see that the results are in a good agreement with the predictions.

4. Nonlinear Evolution Simulation Results

We again use PSC to obtain the results of this section, simulating the full nonlinear evolution of the temperature anisotropy instabilities. First, we start with bi-Maxwellian distributions for both protons and electrons. We choose parameters that are characteristic of the magnetosheath. In particular, the plasma parameters are $T_{p\perp}/T_{p\parallel} = 2.5$, $T_{e\perp}/T_{e\parallel} = 1.5$, $\beta_{p||} = 2$, and $\beta_{e||} = 0.5$. In the magnetosheath, electrons are about 10 times colder than protons. We choose electron temperature to be four times colder because of the limitations of PIC simulations. We need to resolve the electron Debye length, and colder electrons mean smaller electron Debye length which needs finer grid resolutions. We perform two-dimensional PIC simulations. A constant background magnetic field $B_0 = v_A/c = 0.025$ is assumed in the z direction where v_A is the proton Alfven speed and c is speed of light. In the magnetosheath, v_A/c is about 10^{-4}, which would lead to unnecessarily

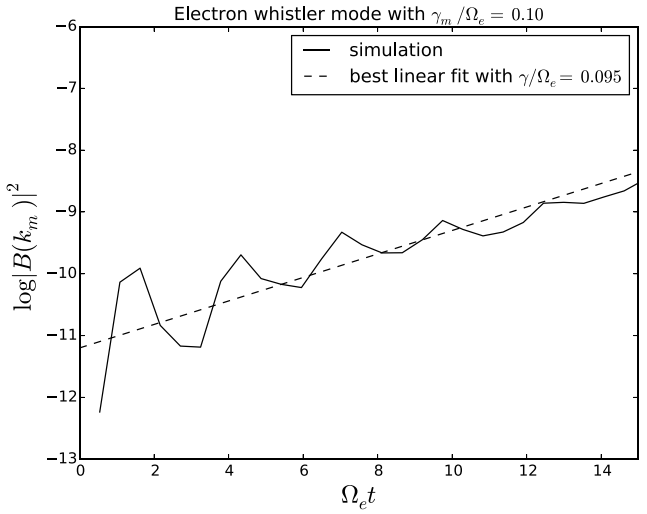

Figure 11. Measured maximum growth rate of electron whistler instability from simulation in the linear regime. The measured growth rate is in agreement with linear dispersion theory prediction.

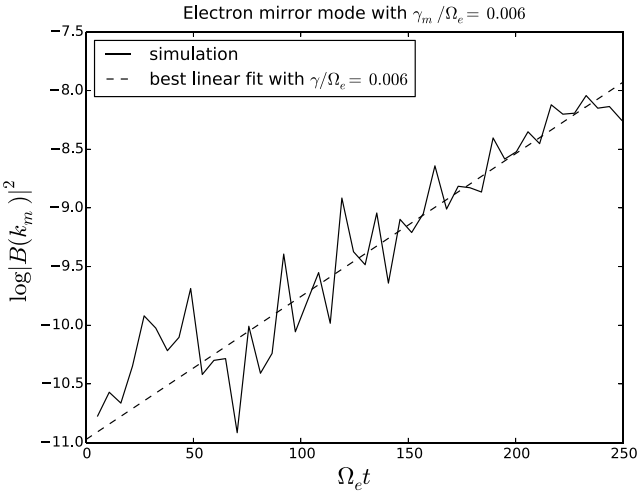

Figure 12. Measured maximum growth rate of electron mirror instability from simulation in the linear regime. The measured growth rate is in good agreement with linear dispersion theory prediction.

small time steps in PIC simulations. We artificially lower the speed of light in our simulations, to make the simulations computationally less expensive. At the same time, we made sure to still keep v_A/c small enough to avoid introducing significant relativistic effects. The number of grid points ($n_y \times n_z$) are 2048×2048. Periodic boundaries are used in each dimension. The number of particles used is on average 200 particles/cell. The size of the grid cells is taken to be $\Delta y = \Delta z = 0.015 d_p$.

For these parameters, linear theory predicts the maximum growth rate of proton cyclotron instability to be $\gamma_m = 0.14\Omega_p$ at $k_m d_p = 0.47$, while the proton mirror instability maximum growth rate is $\gamma_m = 0.10\Omega_p$ with $k_m d_p = 0.53$ at $\theta = 57°$. The electron whistler instability maximum growth rate is $\gamma_m = 0.008\Omega_e$ with $k_m d_e = 0.6$ and $\omega_r = 0.28\Omega_e$.

Since there is an electron temperature anisotropy ($T_{e\perp}/T_{e\parallel} > 1$), the electron whistler instability grows and rapidly isotropizes the electron distribution. Also, the proton cyclotron and the proton mirror instability grow due to the presence of the proton temperature anisotropy ($T_{p\perp}/T_{p\parallel} > 1$).

We choose different mass ratios $m_p/m_e = (25, 100, 400, 1836)$ and examine the electron temperature anisotropy evolution compared to the proton temperature anisotropy changes. Figure 13 shows the dependence of electron temperature anisotropy evolution as a function of proton to electron mass ratio (m_p/m_e)

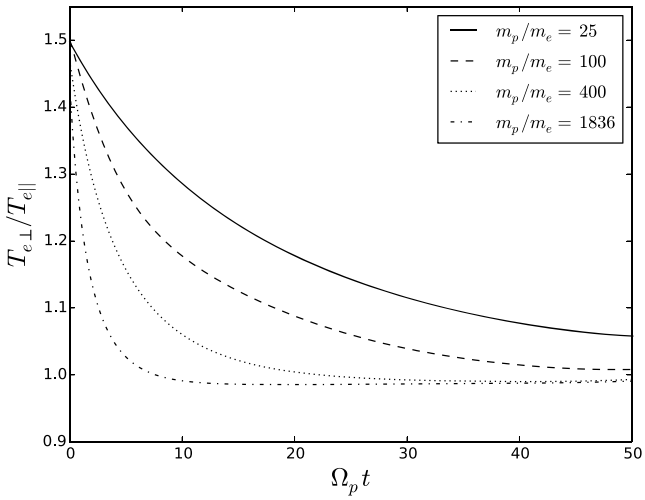

Figure 13. Electron temperature anisotropy evolution for different m_p/m_e. As we increase the mass ratio, the linear regime of electron whistler instability becomes shorter and electrons quickly isotropize.

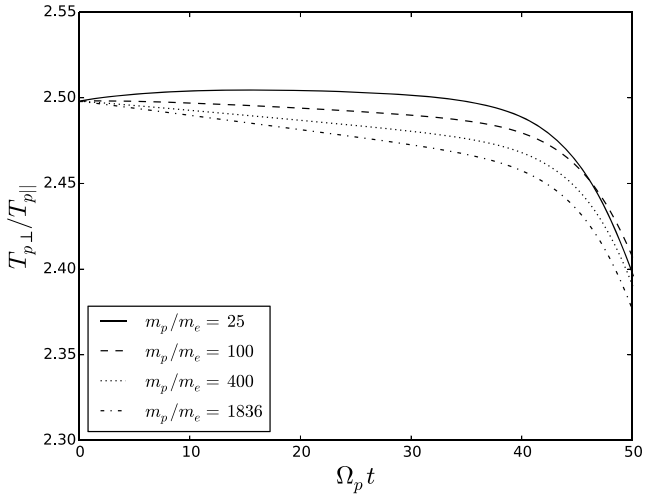

Figure 14. Proton temperature anisotropy evolution for different m_p/m_e. We only show the linear regime of proton instabilities. There is a small unphysical increase in temperature anisotropy for $m_p/m_e = 25$ which is due to the numerical heating.

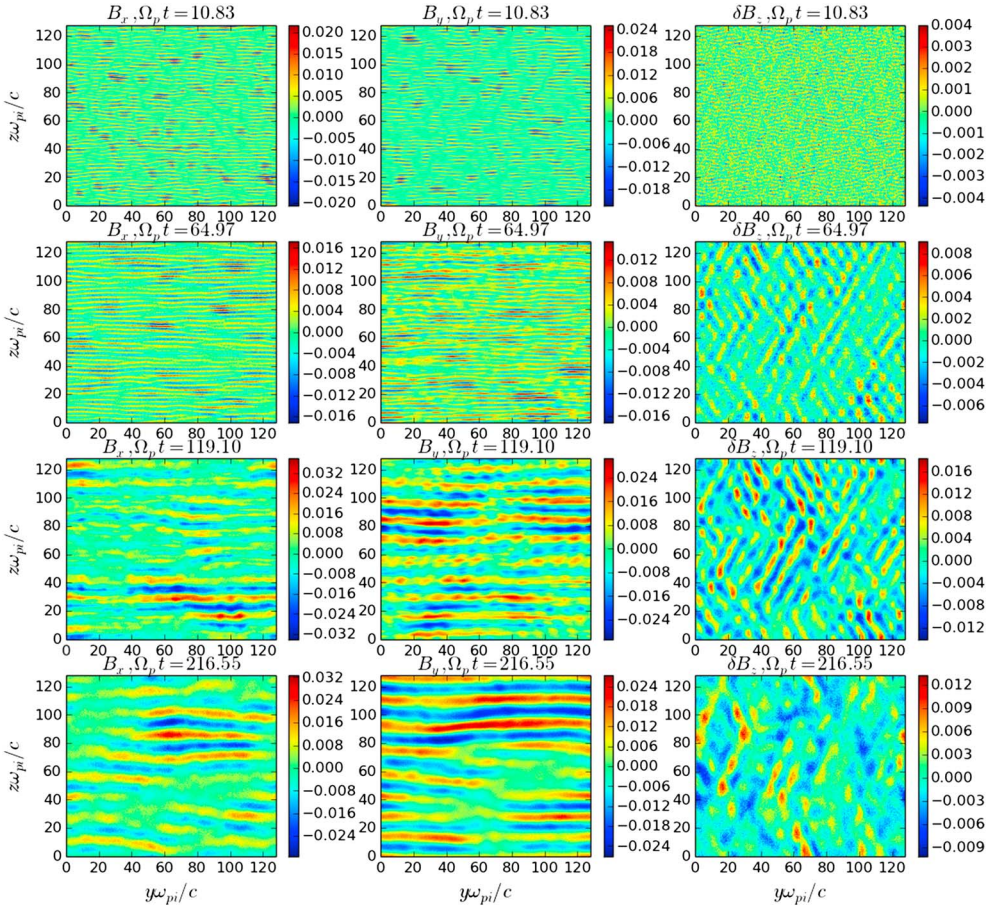

Figure 15. Time evolution of magnetic field components. First column shows B_x, second column shows B_y, and third column is δB_z.

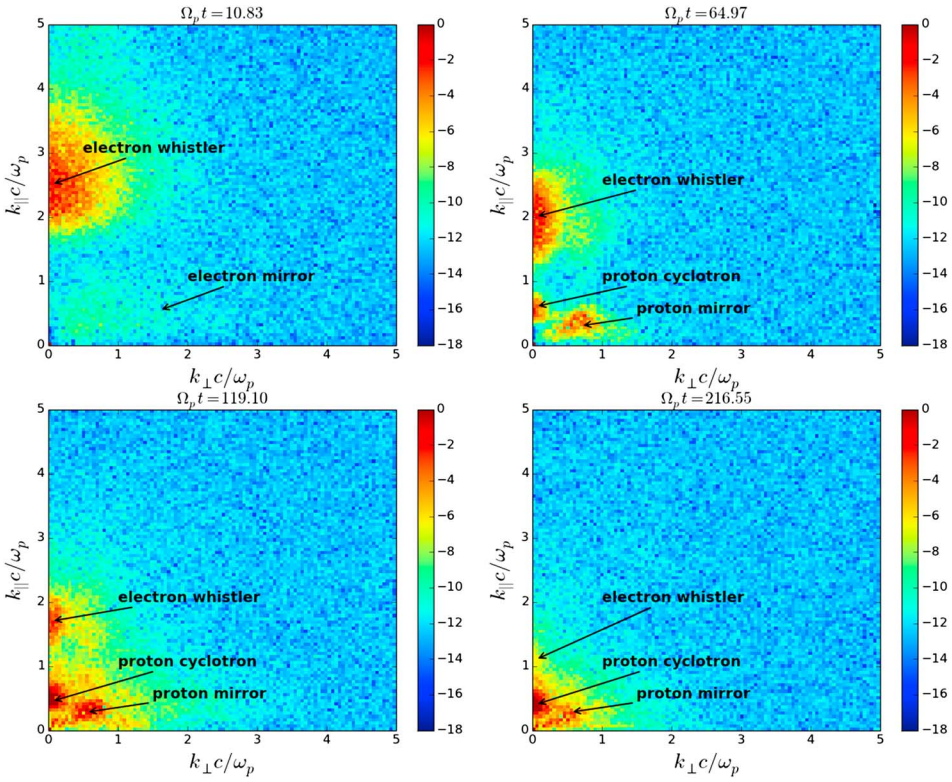

Figure 16. Total magnetic field spectrum. At early time, electron whistler instability is present. Later on, proton cyclotron and proton mirror instabilities grow. As each mode grows nonlinearly, their wavelength becomes larger and their spectrum moves to smaller wave numbers.

in PIC simulations. We only show the linear regime of the proton instabilities which lasts to about $\Omega_p t = 50$ in this case, because we want to see how much electron temperature anisotropy is left when the proton instabilities start to grow nonlinearly. Figure 14 shows the proton temperature anisotropy as a function of time for different m_p/m_e. Figure 13 shows that as we increase the mass ratio, the linear regime of the electron whistler instability becomes shorter since we are making the electrons faster and closer to reality. For $m_p/m_e = 1836$, at the end of proton instabilities linear regime, when proton instabilities start growing nonlinearly, there is no electron temperature anisotropy left for proton mirror instability to take advantage of. So electron anisotropy cannot help the proton mirror mode to dominate over the proton cyclotron instability, unless there is a mechanism that constantly drives the electron temperature anisotropy in the magnetosheath. The adiabatic expansion close to the magnetopause, in the plasma depletion layer, could be a continuous driver of the temperature anisotropies. While the electron distribution isotropizes more slowly at $m_p/m_e = 25$ compared to larger mass ratios, it still leads to essentially isotropic distributions at the end of proton instabilities linear regime.

In order to examine the effects of electron temperature anisotropy on the proton mirror instability in more detail, we perform two simulations with similar parameters and different electron temperature anisotropies. In one simulation we keep electrons isotropic, and in another one, we start with $T_{e\perp}/T_{e||} = 2$. The simulation parameters are $T_{p\perp}/T_{p||} = 2.5$, $\beta_{p||} = 1$, $\beta_{e||} = 1$, $m_p/m_e = 25$, and $B_0 = v_A/c = 0.1$. We use $m_p/m_e = 25$ to keep the computational cost manageable. While we have shown that by the end of the proton linear phase, the electrons have essentially isotropized both at this as well as at the real mass ratio, the artificially lowered mass ratio exaggerated the effects of the electron anisotropy. This is actually helpful as it allows us to more clearly identify the impact on the proton instabilities.

Figure 15 shows the components of the magnetic field at different time steps from the simulation with anisotropic electrons ($T_{e\perp}/T_{e||} = 2$). We can see that at early time steps, electron whistler waves gets excited and are propagating along the background magnetic field. As time goes on, the electron whistler instability saturates and both the proton cyclotron and the proton mirror instability start growing. It is clear that proton

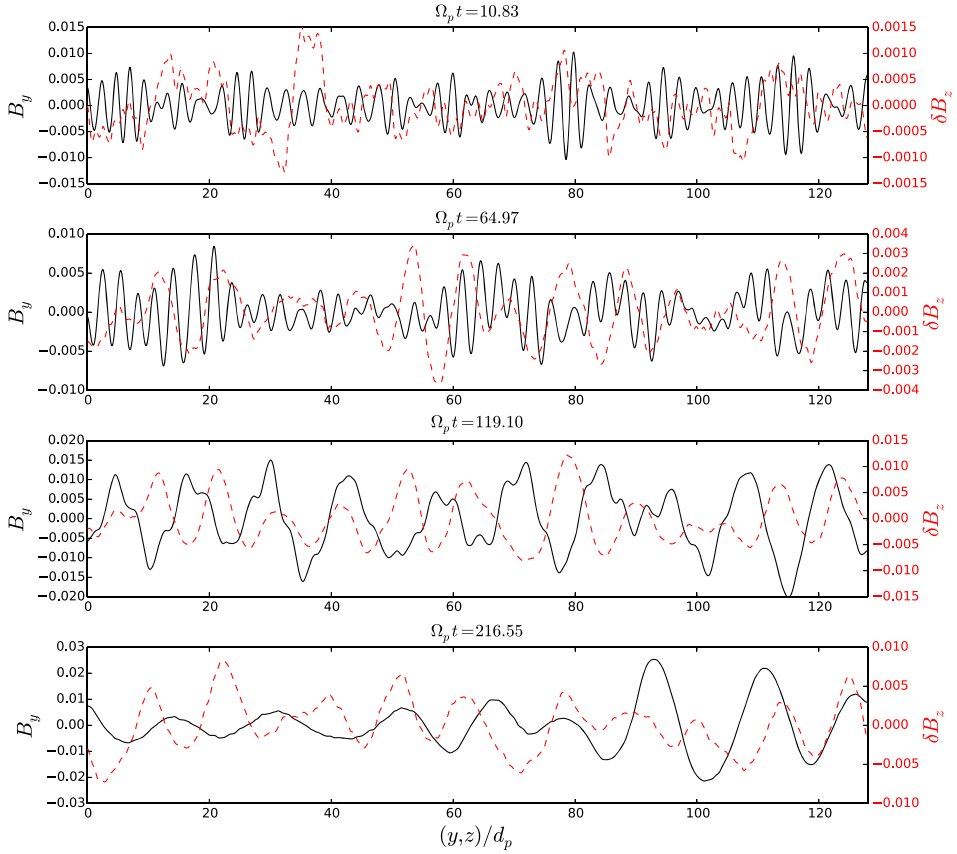

Figure 17. Magnetic field cuts of B_y along z direction at $y = 64d_p$ and δB_z along y direction at $z = 64d_p$ at different times. Black solid line shows B_y and red dashed line is δB_z cut.

cyclotron waves are propagating along the background magnetic field while proton mirror waves are present in the direction oblique to the background magnetic field.

Figure 16 shows the spectrum of the total magnetic field in wave number space at different times. Each instability has been marked in the spectrum in the Figure 16. The electron mirror instability is about 20 times weaker than the electron whistler instability. At early times, the electron whistler instability is the dominant

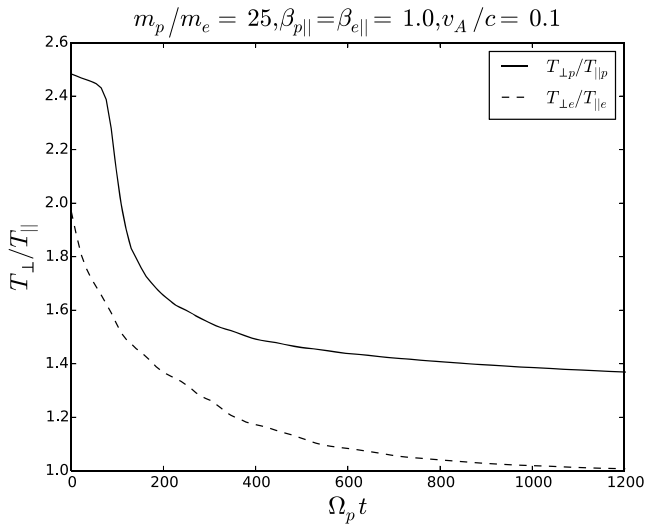

Figure 18. Temperature anisotropy evolution of protons and electrons with $m_p/m_e = 25$.

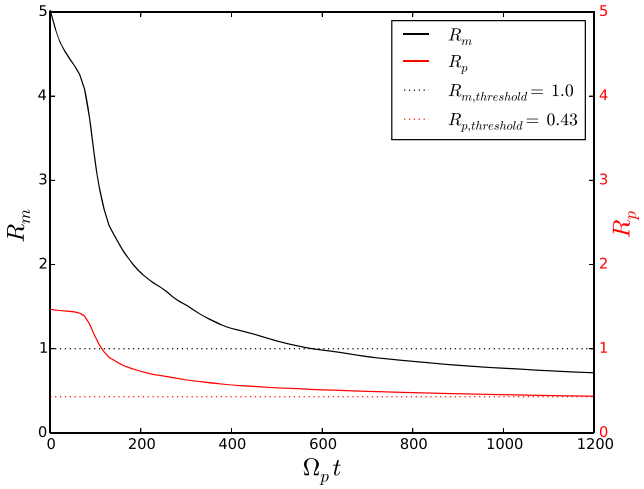

Figure 19. Instability threshold evolution for proton cyclotron instability (red solid line), proton mirror instability (black solid line). The similar color dotted lines show the thresholds for the instabilities.

mode. At later times, the proton cyclotron and the proton mirror instability start growing while the electron whistler instability is still present.

We make cuts in the B_y along z direction at $y = 64d_p$ and in the δB_z along y direction at $z = 64d_p$ from Figure 15. The B_y and δB_z cuts are shown in Figure 17. These cuts resemble the satellite crossings at the locations where these instabilities would typically be present. In Figure 17, we see the electron-scale wavelengths that are electron whistler waves and later, proton-scale wavelength structures grow which are a combination of proton cyclotron and proton mirror mode waves. In the δB_z cuts in Figure 17, the proton-scale structures are proton mirror waves since proton cyclotron waves cannot have perturbations in the direction of the background magnetic field.

In Figure 18, the evolution of proton and electron temperature anisotropy is shown. The proton instabilities start growing nonlinearly around $\Omega_p t = 75$. At this time, the electron temperature anisotropy is still $T_{e\perp}/T_{e\|} = 1.62$. For plasma parameters at this time step, the proton mirror instability is stronger than the proton cyclotron instability. The proton cyclotron maximum growth rate is $\gamma_m/\Omega_p = 0.07$ at $k_m d_p = 0.48$ while

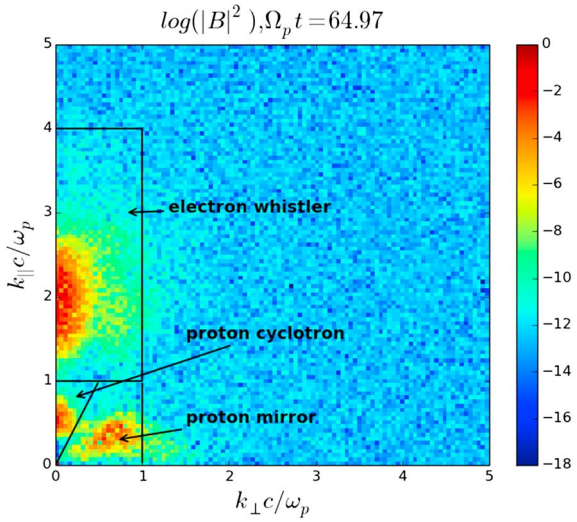

Figure 20. Energy spectrum regions for each instability. Electron whistler instability exist in large $k_{||}$ region and proton cyclotron instability in small $k_{||}$. Proton mirror instability is present in oblique directions with $k_\perp > k_{||}$. Electron mirror instability is very weak and it doesn't contribute in energy density consumption.

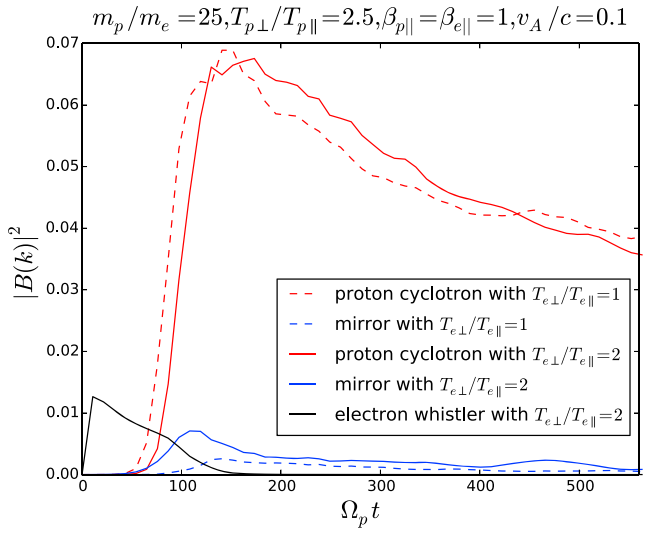

Figure 21. Energy density evolution for different $T_{e\perp}/T_{e\|}$. Solid lines show the energy density of the instabilities with $T_{e\perp}/T_{e\|} = 2$ and dashed lines show the energy density of instabilities with $T_{e\perp}/T_{e\|} = 1$. Solid black line shows the electron whistler instability.

proton mirror instability maximum growth rate is $\gamma_m/\Omega_p = 0.10$ with $k_m d_p = 0.79$ at θ=62°. Then, in the nonlinear regime, both instabilities are present as shown in Figure 16.

In order to see which instability is dominant, we have plotted the instability threshold conditions in Figure 19. The dotted lines in Figure 19 show where the plasma becomes stable for each instability. We see that in the nonlinear regime, the plasma follows the proton cyclotron instability threshold, and this means that proton cyclotron instability is dominant. Figure 21 shows the time evolution of the magnetic energy density of proton cyclotron, proton mirror mode, and electron whistler waves. We measure the magnetic energy density of each wave by filtering the wave spectra for each mode. The wave spectra shows three ranges for wave number vector space as seen in Figure 20. We define the proton cyclotron instability range to be $0 \leq \theta \leq 30°$, and proton mirror instability range is $30° \leq \theta \leq 80°$ for $0 < k_{\perp,||} \leq 1$. For electron whistler instability, we choose $0 \leq \theta \leq 30°$, but the wave number range is $0 < k_\perp \leq 1$ and $1 < k_{||} \leq 4$. We find a significant difference between the saturation levels of the proton cyclotron and the proton mirror instabilities between isotropic and anisotropic electron cases. In the isotropic case, shown in Figure 21 with dashed lines, the magnetic energy density of the proton cyclotron instability is much larger than that of the proton mirror instability. With isotropic electrons, the proton cyclotron instability maximum growth rate is about three times stronger than the proton mirror instability, and we expect proton cyclotron instability to consume most of the available free energy.

In the anisotropic electrons case, the proton mirror instability maximum growth rate is larger than that of the proton cyclotron instability, but we see that the magnetic energy density of the proton cyclotron instability is still more than that of the proton mirror instability. Also, the proton mirror instability gains more magnetic energy density compared to the isotropic electron case, which shows that the electron anisotropy affects the proton mirror instability evolution. At late times, when electrons become isotropic, the instabilities in both simulations saturate at roughly the same magnetic energy density levels. Also, we see that the proton cyclotron instability starts growing at a slightly different time when an electron temperature anisotropy is present, since the presence of an electron temperature anisotropy decreases the proton cyclotron instability growth rate. The proton mirror instability starts growing earlier in the anisotropic electron case, because the electron anisotropy enhances the proton mirror instability growth rate.

5. Summary and Conclusion

In this work, we have investigated the effects of electron temperature anisotropy on the proton mirror instability evolution. Linear theory predicts that presence of an electron temperature anisotropy can enhance the proton mirror instability growth rate, and if it is large enough, it can make the proton mirror instability stronger than the proton cyclotron instability. We showed that anisotropic electrons, however, primarily drive the electron whistler instability. We performed two-dimensional PIC simulations with different electron to proton

mass ratios. We studied how varying the mass ratio affects the electron whistler instability evolution and how it impacts the proton cyclotron and proton mirror instability growth rates. We find that the electron whistler instability consumes the electron-free energy before the proton mirror instability grows into the nonlinear regime, because it grows much faster than the proton temperature anisotropy instabilities. Therefore, all the electron-free energy is gone quickly and has little impact on the much slower proton mirror instability that has barely started growing by that time. Our results show that temperature anisotropy instabilities are sensitive to the chosen mass ratio m_p/m_e in PIC simulations, since an artificial mass ratio can affect the growth and dynamics of the instabilities.

If there is a mechanism in the magnetosheath that keeps $T_{e\perp} > T_{e||}$, it can enhance the proton mirror instability growth rate. For example, the adiabatic expansion in the plasma depletion layer close to the magnetopause makes $T_{e\perp} > T_{e||}$. We will investigate this scenario further in future work.

Acknowledgments
This work was supported by National Science Foundation grant AGS-1056898 and Department of Energy grant DESC0006670. Computations were performed using the following resources: Trillian, a Cray XE6m-200 supercomputer at UNH supported by the NSF MRI program under grant PHY-1229408, and XSEDE resources under contract TG-MCA98N022. Readers interested in attaining the data used should contact the corresponding author at narges.ahmadi@unh.edu.

References

Balikhin, M. A., O. A. Pokhotelov, S. N. Walker, R. J. Boynton, and N. Beloff (2010), Mirror mode peaks: THEMIS observations versus theories, *Geophys. Res. Lett.*, *37*, L05104, doi:10.1029/2009GL042090.

Bavassano-Cattaneo, M. B., C. Basile, G. Moreno, and J. D. Richardson (1998), Evolution of mirror structures in the magnetosheath of Saturn from the bow shock to the magnetopause, *J. Geophys. Res.*, *103*, 11,961–11,972, doi:10.1029/97JA03683.

Burgess, D., E. Mobius, and M. Scholer (2012), Ion acceleration at the Earth's bow shock, *Space Sci. Rev.*, *173*, 5–47, doi:10.1007/s11214-012-9901-5.

Burlaga, L. F., N. F. Ness, and M. H. Acũna (2006), Trains of magnetic holes and magnetic humps in the heliosheath, *Geophys. Res. Lett.*, *33*, L21106, doi:10.1029/2006GL027276.

Chandrasekhar, S. A., A. N. Kaufman, and K. M. Watson (1958), The stability of the pinch, *Proc. R. Soc. A*, *245*, 435–455.

Erdos, G., and A. Balogh (1996), Statistical properties of mirror mode structures observed by Ulysses in the magnetosheath of Jupiter, *J. Geophys. Res.*, *101*, 1–12.

Gary, S. P. (1992), The mirror and ion cyclotron anisotropy instabilities, *J. Geophys. Res.*, *97*, 8519–8529, doi:10.1029/92JA00299.

Gary, S. P., and H. Karimabadi (2006), Linear theory of electron temperature anisotropy instabilities: Whistler, mirror, and Weibel, *J. Geophys. Res.*, *111*, A11224, doi:10.1029/2006JA011764.

Gary, S. P., and M. A. Lee (1994), The ion cyclotron anisotropy instability and the inverse correlation between proton anisotropy and proton beta, *J. Geophys. Res.*, *99*, 11,297–11,301.

Gary, S. P., and J. Wang (1996), Whistler instability: Electron anisotropy upper bound, *J. Geophys. Res.*, *101*, 10,749–10,754, doi:10.1029/96JA00323.

Gary, S. P., S. A. Fuselier, and B. J. Anderson (1993), Ion anisotropy instabilities in the magnetosheath, *J. Geophys. Res.*, *98*, 1481–1488, doi:10.1029/92JA01844.

Gary, S. P., B. Lavraud, M. F. Thomsen, B. Lefebvre, and S. J. Schwartz (2005), Electron anisotropy constraint in the magnetosheath: Cluster observation, *Geophys. Res. Lett.*, *32*, L13109, doi:10.1029/2005GL023234.

Génot, V., E. Budnik, C. Jacquey, I. Dandouras, and E. Lucek (2009), Mirror modes observed with Cluster in the Earth's magnetosheath: Statistical study and IMF/solar wind dependence, in *Advances in Geosciences, Solar Terrestrial (ST)*, vol. 14, edited by M. Duldig, p. 263, World Sci., Singapore.

Germaschewski, K., W. Fox, N. Ahmadi, L. Wang, S. Abbott, H. Ruhl, and A. Bhattacharjee (2013), The plasma simulation code: A modern particle-in-cell code with load balancing and GPU support, arXiv:1310.7866.

Hasegawa, A. (1969), Drift mirror instability in the magnetosphere, *Phys. Fluids*, *12*, 2642.

Hellinger, P., and P. M. Trávnícek (2005), Magnetosheath compression: Role of characteristic compression time, alpha particle abundance, and alpha/proton relative velocity, *J. Geophys. Res.*, *110*, A04210, doi:10.1029/2004JA010687.

Joy, S. P., M. G. Kivelson, R. J. Walker, K. K. Khurana, C. T. Russell, and W. R. Paterson (2006), Mirror mode structures in the Jovian magnetosheath, *J. Geophys. Res.*, *111*, A12212, doi:10.1029/2006JA011985.

Kaufmann, R. L., J. T. Horng, and A. Wolfe (1970), Large-amplitude hydromagnetic waves in the inner magnetosheath, *J. Geophys. Res.*, *75*, 4666–4676.

Kennel, C. F., and H. E. Petschek (1966), Limit on stably trapped particle fluxes, *J. Geophys. Res.*, *71*, 1–28.

Masood, W., and S. J. Schwartz (2008), Observations of the development of electron temperature anisotropies in Earth's magnetosheath, *J. Geophys. Res.*, *113*, A01216, doi:10.1029/2007JA012715.

Midgeley, J. E., and L. Davis Jr. (1963), Calculation by a moment technique of the perturbation of the geomagnetic field by the solar wind, *J. Geophys. Res.*, *68*, 5111–5123.

Pantellini, F. G. E., and S. J. Schwartz (1995), Electron temperature effects in the linear proton mirror instability, *J. Geophys. Res.*, *100*, 3539–3549, doi:10.1029/94JA02572.

Pokhotelov, O. A., M. A. Balikhin, H. S.-C. K. Alleyne, and O. G. Onishchenko (2000), Mirror instability with finite electron temperature effects, *J. Geophys. Res.*, *105*, 2393–2402.

Pokhotelov, O. A., O. G. Onishchenko, M. A. Balikhin, R. A. Treumann, and V. P. Pavlenko (2001), Drift mirror instability in space plasmas: 2. Nonzero electron temperature effects, *J. Geophys. Res.*, *106*, 13,237–13,246.

Pokhotelov, O. A., R. A. Treumann, R. Z. Sagdeev, M. A. Balikhin, O. G. Onishchenko, and V. P. Pavlenko (2002), Linear theory of the mirror instability in non-Maxwellian space plasmas, *J. Geophys. Res.*, *107*(A10), 1312, doi:10.1029/2001JA009125.

Porazik, P., and J. R. Johnson (2013a), Linear dispersion relation for the mirror instability in the context of the gyrokinetic theory, *Phys. Plasmas*, *20*, 104501.

Porazik, P., and J. R. Johnson (2013b), Gyrokinetic particle simulation of nonlinear evolution of mirror instability, *J. Geophys. Res. Space Physics*, *118*, 7211–7218, doi:10.1002/2013JA019308.

Price, C. P., D. W. Swift, and L. C. lee (1986), Numerical simulation of nonoscillatory mirror waves at the Earth's magnetosheath, *J. Geophys. Res.*, *91*, 101–112.

Remya, B., R. V. Reddy, B. T. Tsurutani, G. S. Lakhina, and E. Echer (2013), Ion temperature anisotropy instabilities in planetary magnetosheaths, *J. Geophys. Res. Space Physics*, *118*, 785–793, doi:10.1002/jgra.50091.

Russell, C. T., W. Riedler, K. Schwingenschuh, and Y. Yershenko (1987), Mirror instability in the magnetosphere of Comet Halley, *Geophys. Res. Lett.*, *14*, 644–647.

Scharer, J. E., and A. W. Trivelpiece (1967), Cyclotron wave instabilities in a plasma, *Phys. Fluids*, *10*, 591.

Shoji, M., Y. Omura, B. T. Tsurutani, O. Verkhoglyadova, and B. Lembege (2009), Mirror instability and L-mode electromagnetic ion cyclotron instability: Competition in the Earth's magnetosheath, *J. Geophys. Res.*, *114*, A10203, doi:10.1029/2008JA014038.

Soucek, J., E. Lucek, and I. Dandouras (2008), Properties of magnetosheath mirror modes observed by Cluster and their response to changes in plasma parameters, *J. Geophys. Res.*, *113*, A04203, doi:10.1029/2007JA012649.

Southwood, D. J., and M. G. Kivelson (1993), Mirror instability: 1. Physical mechanism of linear instability, *J. Geophys. Res.*, *98*, 9181–9187.

Stix, T. H. (1962), *The Theory of Plasma Waves*, McGraw-Hill, New York.

Tsurutani, B. T., E. J. Smith, R. R. Anderson, K. W. Ogilvie, J. D. Scudder, D. N. Baker, and S. J. Bame (1982), Lion roars and nonoscillatory drift mirror waves in the magnetosheath, *J. Geophys. Res.*, *87*, 6060–6072.

Tsurutani, B. T., G. S. Lakhina, O. P. Verkhoglyadova, E. Echer, F. L. Guarnieri, Y. Narita, and D. O. Constantinescu (2011), Magnetosheath and heliosheath mirror mode structures, interplanetary magnetic decreases, and linear magnetic decreases: Differences and distinguishing features, *J. Geophys. Res.*, *116*, A02103, doi:10.1029/2010JA015913.

Winterhalter, D., M. Neugebauer, B. E. Goldstein, E. J. Smith, S. J. Bame, and A. Balogh (1995), Ulysses field and plasma observations of magnetic holes in the solar wind and their relation to mirror-mode structures, *J. Geophys. Res.*, *99*, 23,371–23,381.

Seough, J., and P. H. Yoon (2013), Solar wind proton anisotropy versus beta relation, *Phys. Rev. Lett.*, *110*, 071103, doi:10.1103/PhysRevLett.110.071103.

Zwan, B. J., and R. A. Wolf (1976), Depletion of solar wind plasma near a planetary boundary, *J. Geophys. Res.*, *81*, 1636–1648.